Rock and Soil Mechanics

Volume 42 | Issue 12 Article 2

2-28-2022

Mechanical properties and failure mechanisms of the rocklike specimens under tension shear effects

Chao-biao ZHOU
School of Civil Engineering, Wuhan University, Wuhan, Hubei 430072, China

Dong LIU
Power China Zhongnan Engineering Corporation Limited, Changsha, Hunan 410014, China

Qing-hui JIANG
School of Civil Engineering, Wuhan University, Wuhan, Hubei 430072, China, jqh1972@yahoo.com.cn

Custom Citation

ZHOU Chao-biao, LIU Dong, JIANG Qing-hui. Mechanical properties and failure mechanisms of the rocklike specimens under tension shear effects[J]. Rock and Soil Mechanics, 2021, 42(12): 3335-3344.

Rock and Soil Mechanics 2021 42(12): 3335−3344 ISSN 1000−7598
https: //doi.org/10.16285/j.rsm.2021.5520 rocksoilmech.researchcommons.org/journal

Mechanical properties and failure mechanisms of the rocklike specimens under tension shear effects

ZHOU Chao-biao[1], LIU Dong[2], JIANG Qing-hui[1]
1. School of Civil Engineering, Wuhan University, Wuhan, Hubei 430072, China
2. Power China Zhongnan Engineering Corporation Limited, Changsha, Hunan 410014, China

Abstract: Using self-designed tension shear auxiliary device, we carried out a tension shear test and a compression shear test under different normal stresses between −0.28 and 3.0 MPa. We applied the acoustic emission to compare and analyze the mechanical properties and the damage failure mechanisms of the specimens for both tests. The main results are listed as below. The tension shear auxiliary device can help carry out the tension-shear test well. The peak stress varies non-linearly with the normal stress and is more sensitive to the normal tensile stress. The Hoek-Brown strength criterion can generally characterize the strength of the full stress area. The post-peak stress of the specimen in tension shear test drops severely and separates into two parts rapidly, showing the failure characteristics with more brittleness than that of the compression shear test. The morphological characteristics of the fracture plane are closely related to the direction and magnitude of normal stress. For compression shear test, the damage degree represented by the acoustic emission parameters is greater, as well as the failure degree of the fracture plane, compared with those observed in tension shear test. The frictional area and the local spalling of the fracture plane are also more obvious for the specimens in compression shear test, compared with those in tension shear test. As the normal stress increases, the duration of the acoustic emission quiet period gets longer, and the start time of the unstable crack propagation gets later. Compared with the compression one, the tension shear test shows a shorter duration time for each stage of the failure process as well as a higher failure rate. The critical points σ_{cc}、σ_{ci} and σ_{cd} of the shear-stress plot and the acoustic emission parameters can represent, respectively, the macroscopic and microscopic failure process of the specimen. The critical point σ_{cd} and the acoustic emission b value can be used as omens of rock failure.

Keywords: tension shear test; strength criterion; brittle failure; acoustic emission; damage failure mechanism; omen

1 Introduction

According to the critical stress in the failure process of rocks, the failure modes can be classified into three types: tension failure, shear-compression failure and tension-shear failure. Increasing studies have shown that tensile stress commonly exists in rocks. In most cases, rocks are in tensile or tensile shear stress states. For example, in the high steep rock slopes or deep underground caves, tensile stress will be generated in the disturbance zone of the rocks due to the excavation unloading[1−2]. Therefore, it is important to have the in-depth studies of the failure mechanism of rock mass under tensile and shear stress.

In early years, there were insufficient studies worldwide on the state of rock mass under tensile stress and shear stress due to the lack of lab equipment. Most of those studies used indirect or direct tensile experiments to study the tensile properties of rocks. Li et al.[3] and Yu et al.[4−5] studied the elastic modulus, Poisson's ratio and other mechanical properties of rocks under direct tension and compression effect. Ramsey et al.[6] used a dog-bone-shaped marble specimen that is thin at the middle and thick at both ends to evaluate the tensile shear strength of the rock. The test results show that the specimen exhibits tensile shear failure and the transition from tensile crack to shear crack. However, this method has not been applied widely mainly due to the limitation of the shape of the specimen and the lab device. In addition, Zhou et al.[7] conducted the on-site tensile shear tests on the slope of the Three Gorges Ship Lock and discovered the nonlinear relationship between the tensile shear strength and the normal stress. The findings are new to the tensile shear strength criterion. Kong et al.[8−9] used the latest compression-shear clay-strength theory and showed the cutoff points between tension-shear and compression-shear failure of saturated clay through a comparative analysis. They established a tensile-shear coupling strength model for saturated clay. The limit of their work is mainly the lack of corresponding testing data to verify the bi-directional and three-directional tensile strength.

In recent years, Huang et al.[10−13] used a self-designed tensile-shear device to study the shear behavior of rock under tensile shear stress. They analyzed the characteristics of rock deformation, rock strength, as well as fracture surface. The study indicated that the Hoek-Brown strength criterion can be used to characterize well the tensile and shear strength of the rock. Chen et al.[14] carried out uniaxial tensile tests, as well as tensile shear and compressive shear tests to study the microscopic failure mechanism of rocks.

Received: 9 April 2021 Revised: 15 July 2021
The work was supported by the National Natural Science Foundation of China(51769014).
First author: ZHOU Chao-biao, male, born in 1996, M.Sc. majoring in numerical method of geotechnical mechanics. E-mail: 2019202100017@whu.edu.cn
Corresponding author: JIANG Qing-hui, male, born in 1972, PhD, Professor, PhD supervisor, mainly engaged in the teaching and research on numerical methods of geotechnical mechanics. E-mail: jqh1972@yahoo.com.cn

They used Scanning Electron Microscope (SEM) to analyze the failure mechanism and crack evolution process of mineral crystals, and presented a relationship between the macro-failure of the rock and its micro-crack evolution mechanism.

Most recent studies focus on the deformation mechanism and the mechanical properties by using the tensile shear experiments. However, the failure characteristics of the specimen are less recorded and studied during the experiment. Acoustic emission (AE) signals can characterize the deterioration and failure of rocks and concrete during an experiment. The method can be used to monitor the internal holes, cracks development and the penetration between internal and external cracks. Meng et al.[15−16] used AE to record the failure process of rocks during the uniaxial periodic compressional loading tests. They showed the relationship between AE signals and the evolution of rock internal energy. Li et al.[17] used white marble under direct tensile tests and analyzed the dominant frequency and waveforms of the AE signals. They showed the relationship between the dominant frequency and the microscopic failure mechanism of the rock. Cheon et al.[18] proposed a metric to evaluate the failure type and the damage degree of the rocks based on the parameters of AE, and used this method to monitor and evaluate the degree of shear failure of rock slopes. Meng et al.[19] used AE events to analyze the failure of granite in shear tests. They showed the relationship between the rough damage and the shear behavior of the joints. In addition, they used the cumulative number of the AE events to classify the stages of damage in the shearing process. Zhang et al.[20] and Liu et al.[21] studied the damage evolution process of rock under the uniaxial compression. They used AE characteristic parameters to classify the damage evolution stages and established models for the development of rock damage.

As shown by the review, there are insufficient studies on the tensile-shear effect, especially the rock failure characteristics during the experiments. In this study, we used self-designed tension-shear auxiliary device to carry out experimental shear and tension tests. We studied the mechanical properties of the specimen under tensile and shear stress, and extended the yield strength criterion to the full stress zone, rather than the compression shear zone. We used the AE to monitor the initiation and propagation of cracks during the test, which illustrates the damage evolution of the specimen as well as its inherent damage mechanism.

2 Experiments

2.1 Equipments

2.1.1 The design of tensile shear auxiliary device

Figure 1 shows the self-designed tension shear auxiliary device. It mainly consists of two portal frames, two U-shaped parts, two T-shaped shearing heads, two types of bolt, and a chute.

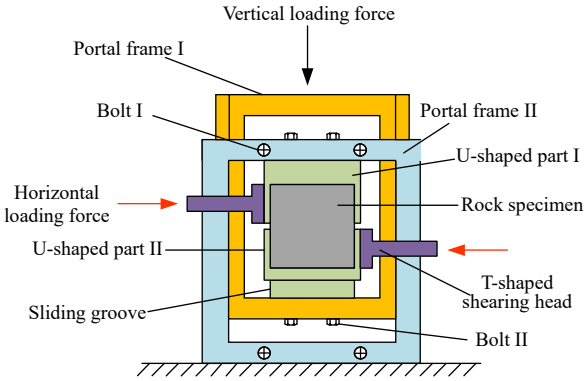

Fig. 1 Schematic illustration of the tension shear auxiliary device

The two portal frames form the main body of the device. There are protruding sliding bars on the left and the right hand sides of the portal frame I, whereas there are two same parts and sliding grooves at the front and the rear of the portal frame II. The two frames are fitted to each other by the sliding groove and the sliding bar; and they are fixed by bolt I. The use of bolt ensures that under a vertical load, the device movement can also be purely vertical, which reduces the effect of eccentric force. Lubricant is needed at the joint between the sliding groove and the sliding bar to reduce the effect of the friction.

The two U-shaped parts are glued on both the top and bottom of the rock specimen by a strong epoxy resin. The U-shaped part II is connected with the lower sliding groove to ensure the rock specimen is free to move along the horizontal direction. The U-shaped part I and the sliding groove are connected to the portal frame by bolts II, which can convert the vertical pressure loaded on the portal frame I into tensile force and act on the rock specimen. The T-shaped shearing head uses the direct shear device to apply the tangential stress as required.

The parts of the device are straightforward to use and assemble. It can convert the vertical pressure on the rock specimen into tensile stress and then apply the tangential stress by a shearing device to achieve the tensile-shear effect.

2.1.2 The direct shear device YZW50

A direct shear device YZW50 was used to conduct the experiment. The normal pressure is no more than 500 kN, and the normal working stroke is 200 mm; the tangential pressure is no more than 500 kN, and the tangential working stroke is 200 mm. The tangential speed is within the range between 0.1 and 20 kN /s. The device has a displacement meter with the accuracy of 0.001 mm.

2.1.3 The AE system AMSY-6

We used the AMSY-6 system produced by Vallen, which is a fully digital AE system with full waveforms of signals. It can monitor the internal structural changes of materials as well as the release of energy, plus a variety

of industrial applications. In our experiment, the threshold of the acoustic acquisition is 40 dB. The pre-amplification is 40 dB. The sensor ID is VS45-H, whose response frequency has the range between 40 to 450 kHz. The resonant frequency is 280 kHz.

2.2 Specimen preparation

We used water, grade 42.5 Portland cement and fine sand (particle size less than 1 mm) as raw materials according to Chen et al.[22−23]. We weighed the raw materials following the ratio of 1∶2∶4, mixing the cement with the fine sand uniformly first and pour it into a mixer where water comes in. The prepared cement mortar was poured into a customized steel mold with a size of 60 mm× 60 mm×60 mm. The mortar was vibrated and compacted, and then still for 24 hours. After demolding, the specimen was placed indoor with curing by water. In order to ensure the mechanical and physical properties, all the specimens were cured for 28 days before the test, as shown in Fig.2(a).

(a) Cement mortar specimens

(b) Specimen cementation

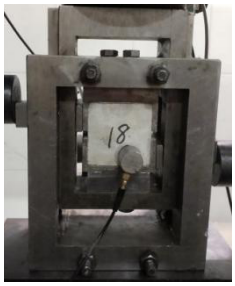

(c) Layout of the AE sensors

Fig. 2 Specimen curing and the layout of the tension shear auxiliary device

We notice the fact that the heterogeneity and the diversity of the cement mortar can be relatively severe. Therefore, we measured the P-wave velocity and the density for each specimen after the water curing. And we use those specimens with similar velocity and density for testing, so as to minimize the error caused by the specimens themselves.

The measurement of the mechanical parameters is described as follows. We applied uniaxial compression tests and direct tension tests to the cylindrical specimens that were made under the same conditions. We repeated each test three times and took the mean value. According to the tests, the uniaxial compressive strength of the specimen is 38.6 MPa. The elastic modulus is 18 GPa. The uniaxial tensile strength is 1.2 MPa and the density is measured as 2.56 g /cm^3. The parameters of the artificial specimens are similar to those of the natural rocks, which can therefore be used to provide a reference for those experiments using natural rocks.

2.3 Specimen installation and test workflow

The test aims to analyze the mechanical properties and damage mechanisms of the specimen under tensile and shear stress, including the specimen behaviors under different normal tensile stress, as well as the comparative analysis of the results between tensile shear and compression shear tests.

Figure 2(b) shows the specimen and the U-shaped part of the tensile-shear auxiliary device. The adhesive is a strong epoxy resin with an anti-tensile strength of 30 MPa. The adhesive reaches its maximum strength after 24 hours of bonding. The AE sensor is placed 5 mm below the shear surface of the specimen, as shown in Fig.2(c).

Figure 3 shows the layout of the experiment. The YZW50 direct shear device was used to conduct the tensile shear test, with the tensile shear auxiliary device. The maximum vertical and horizontal loads are both 500 kN. During the test, we first placed the AE sensor and ensured the signals could be successfully collected. Then the device applied the normal load with the increasing speed of 0.05 kN /s until the force reaches the designed value. Next, the device applied a shear stress at a shear displacement rate of 0.3 mm /min until the failure occured. The deformation of the specimen and the stress data were recorded by the direct shear device throughout the test. The normal stresses are −0.28, −0.42, −0.56, 0.50, 1.00, 2.00, 3.00 MPa, respectively, where the negative normal stress indicates the tensile stress.

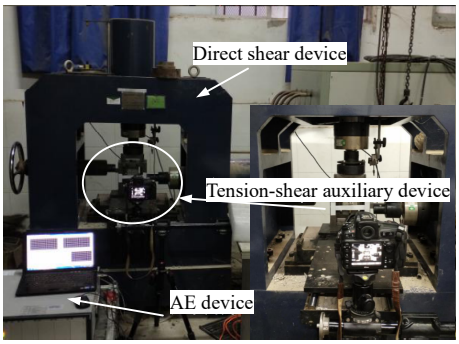

Fig. 3 The direct shear device installed with the tension-shear auxiliary device plus the AE device

3 Results and analysis

3.1 Deformation characteristics

Figure 4 shows the stress−displacement plots under tension and compression shear tests with different normal stresses. There are obvious differences between tension shear and compression shear according to Fig.4. Compared to compression shear, the plot in tension shear test shows no residual stage after reaching the peak. The main reason

is that under the normal tensile stress, the specimen is quickly pulled apart after shearing and breaking into two parts. In addition, the peak displacement (the displacement corresponding to the peak stress) in tensile shear test is smaller than that in the compression shear test. It decreases with the increase of the normal tensile stress.

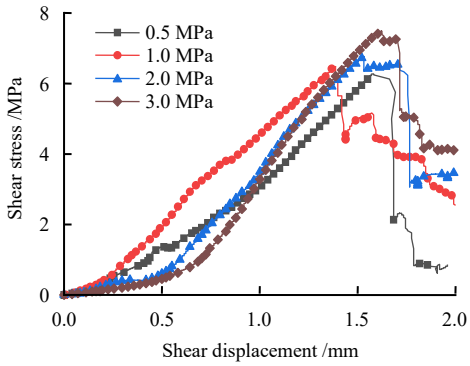

(a) The shear stress−displacement plot in compression shear test

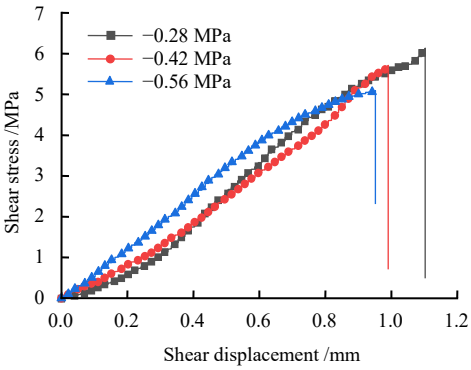

(b) The shear stress−displacement plot in tension shear test

Fig. 4 The shear stress−displacement plots in tension and compression shear tests under different normal stresses

As shown in Fig.4(b), the stage of initial crack closure in tensile shear test is different from that in compression shear test. In addition to the crack closure caused by shear stress, it also includes crack opening caused by normal tensile stress. This observation is consistent with the conclusion shown by Huang et al.[10]. Therefore, compared to the compression shear, the plot in tensile shear test shows less fluctuation and is slightly concave. After reaching the peak, the stress drops rapidly and even approaches to zero. Compared with the residual stage that shown by the post-peak variation presented in the compression shear test, the brittleness of the rock is greater under the tensile shear stress.

3.2 Characteristics of the fracture plane

The failure process of the specimen under tensile shear stress is shown in Fig.5. The photographs taken by a high-speed camera show the outcome of the specimens before and after the failure process. The tangential displacements in the photographs are 0.5 mm, 0.8 mm, and 1.0 mm, respectively. The specimen is damaged within a short time, accompanied by an AE of 'bang'. As shown by Fig.5, no obvious cracks appeared in the specimen during the shearing process. This indicates that under normal tensile stress, the cracks connection of the specimen quickly develops after the initiation of the shear cracks. This is consistent with the "greater brittleness" observation that found by the tensile shear displacement-stress plots.

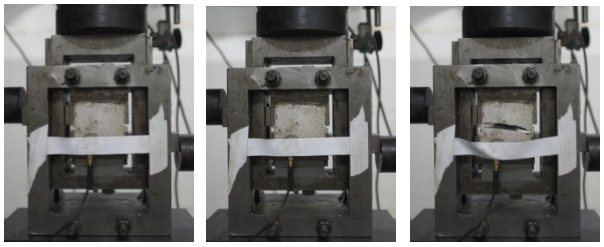

Fig. 5 The failure process of the specimen in tension shear test

The fracture path on the plane of the specimen is shown in Fig.6. The failures of specimens all extend along the pre-determined shear plane and around its vicinity. The angle between the fracture plane and the horizontal plane is slightly larger in compression shear test compared to that in tensile shear test. Local spalling of the fracture plane can be observed in both the two tests. As the normal compressive stress increases, local spalling becomes more severe as shown by the compression shear tests. In contrast, the change of spalling is not obvious with the increase of normal tensile stress, as shown by the tensile shear tests.

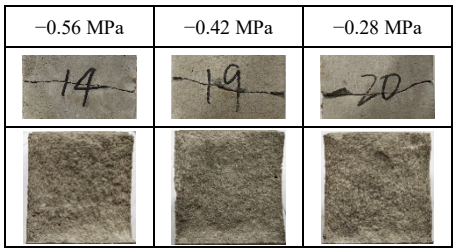

(a) Normal tension

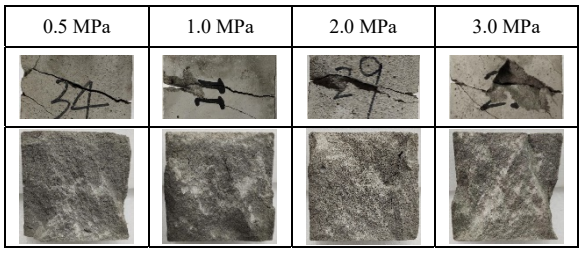

(b) Normal compression

Fig. 6 Fracture paths and the morphology of the fracture plane

The outcome of the fracture plane of the specimen is shown in Fig.6. The photos are selected from the lower part of the rock mass. Fig.6(a) shows the fracture planes of the specimens from the tensile shear test. The larger the normal tensile stress, the smaller the roughness of the fracture plane, according to Fig.6(a). In addition, there is no friction zone on the fracture planes from the tensile shear test. The main reason is that under normal tensile

stress, the specimen quickly separates into two halves after shearing and the process is barely affected by the sliding friction. For the compression shear test, the friction area of the fracture plane is relatively smooth, as shown by the white area in Fig.6(b). The smoothness is caused by the friction between the upper and lower surfaces of the broken specimen. In addition, the area of the friction zone increases with the increase of the normal compressive stress. Therefore, the area can be used to characterize the damage degree of the specimen. The larger the area of the friction zone is, the greater the degree of damage becomes.

The observations above demonstrate that the failure of the rock is closely related to the direction and magnitude of the normal stress. The damage of the specimens under normal compression is more severe than the specimens under normal tension, which indicates that the direction of the normal stress has significant impacts on the formation of the fracture plane. In addition, the greater the normal compression is, the greater the damage degree of the specimen becomes, which means the magnitude of the normal stress affects the damage degree of the rock.

3.3 Characteristic of strength

Figure 7 shows the plots of peak shear stresses versus the normal stresses. As shown by the figure, the peak shear strength of the specimen increases with transition of the normal stress from tension to compression. By comparing the slope of the plot within the tensile and the compressional stage, it shows the peak shear strength of the specimen is more sensitive to the normal tensile stress. Therefore, it is significant in practical engineering to study the impact of tension or tension shear stress on the interested rock mass.

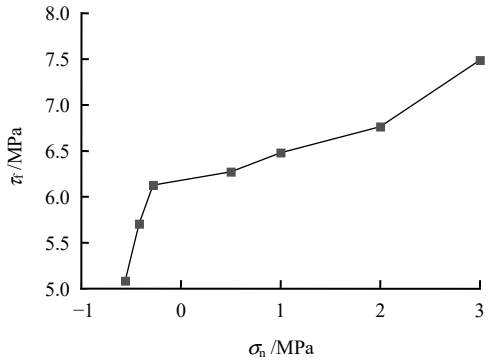

Fig. 7 Plot of the peak shear stress versus the normal stress

Most existing experimental research obtain the strength criterion based on the compression shear test results. After that, the fitted results from the compression shear test are extended to the tensile shear stress, which yields the strength envelope covering the full stress area. Li et al.[24] considered the Drucker-Prager criterion as the strength yield criterion for the compression shear. For the tension shear, they proposed two schemes to extend the D-P criterion: using a spherical yield surface and using a hyperbolic rotation surface, respectively, to replace the original D-P cone surface. However, the derivation is complicated and has not yet been verified. Zhou et al.[25] used the self-designed lab device and collected the tensile shear test data. They used a parabolic strength criterion to fit the data, and the results are decent on the full stress area. Nevertheless, the accuracy is not outstanding considering specifically the tension shear area or when the normal compression stress is low.

Generally speaking, the extrapolation of the strength criterion from the compression shear to the tension shear may not be robust and transferrable. For example, extrapolating the Mohr-Coulomb strength criterion to the tensile stress will overestimate the actual tensile and shear strength[9, 14, 26–27]. Therefore, it is more accurate to analyze the full stress modelling by using both the tensile shear and compression shear test data.

As discussed above, the Mohr-Coulomb and Hoek-Brown strength criteria was used to fit all the test data under different normal stresses to determine the fitting parameters, as shown in Eqs. (1) and (2).

(1) Mohr-Coulomb strength criterion

$$\tau_{\mathrm{f}} = \sigma_{\mathrm{n}} \tan\varphi + c \tag{1}$$

(2) Hoek-Brown strength criterion

$$\tau_{\mathrm{f}} = A(\sigma_{\mathrm{n}} + \sigma_{\mathrm{t}})^{B} \tag{2}$$

Figure 8(a) shows the fitting results based on the Mohr-Coulomb strength criterion. The fitting has the accuracy measured as R^2 = 0.869, with a root mean square error (RMSE) of 0.256. The resultant model overestimates the tensile shear strength in the tensile stress area, and lacks the ability to fit to the tensile stress area. The overall fitting quality is not satisfying. Fig.8(b) shows the fitting results using the Hoek-Brown strength criterion. The fitting has the accuracy measured as R^2 = 0.912, with a RMSE of 0.210. The fitting is meaningful in the tensile stress area, and the resultant model can generally better capture the strength characteristics for the full stress area.

3.4 Characteristics of AE parameters

The AE technology was used to monitor the initiation, propagation and penetration of the internal cracks inside the specimen. Through the analysis of the AE parameters including hit, energy, and amplitude, we obtain the evolution of the damage degree of the specimen. As shown in Fig.9, we select the examples under a normal tensile stress of 0.42 MPa and a compressive stress of 3 MPa. We present the relationship between the shear stress and the AE parameters (hit rate, energy rate, and normalized cumulative number of hits).

Figures 9(a) and 9(b) show the variation under varied normal compressive stresses. Before reaching the peak stress, the hit rate increases with the shear stress and the

magnitude is low. At around the peak stress, the hit rate increases sharply and reaches the peak hit rate. In the post-peak residual stage, the hit rate drops sharply and remains stable at a relatively low level, which is consistent with the post-peak stress curve. The change of energy rate with shear stress is similar to the trend of hit rate, that is, both the energy and the number of hit increase sharply. This may be owing to the local cracking and spalling of the specimen during the compression and shearing process, which is similar to the results obtained by Meng et al.[19, 28]. The normalized cumulative number of hits is the ratio of the cumulative number of hits at every time step to the total number of hits. It can integrate the curves of the specimen under different normal stresses and can reflect the damage degree of the specimen at every moment.

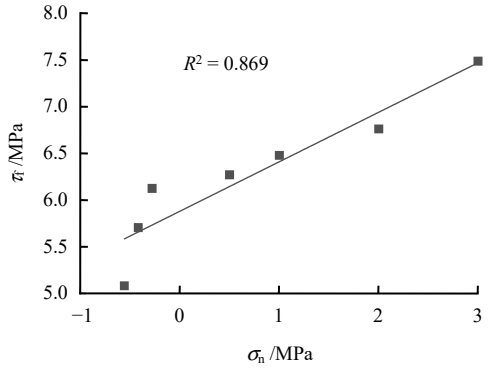

(a) Mohr-Coulomb strength criterion

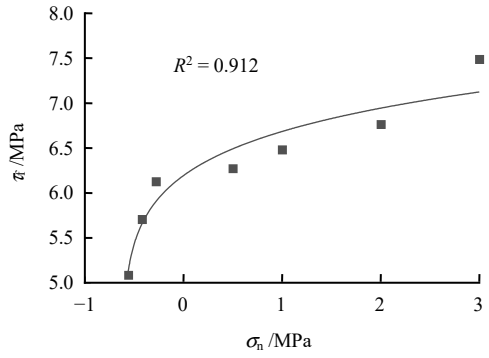

(b) Hoek-Brown strength criterion

Fig. 8 Fit of the strength failure criteria to the test data

Figures 9(c) and 9(d) show the variation under normal tensile stress. The hit rate and the energy rate under normal tensile stress show the similarities to those under normal compressive stress. The difference is mainly the lack of the post-peak phase. The hit rate plot shows its continuous increase with the increase of shear stress during the test. Until the failure, the hit rate remains at a high level. The stress drops abruptly after the appearance of the shear fracture of the specimen. The analysis above shows that the specimen under normal tensile stress owns the characteristics of brittle failure.

The plots of Figs. 9 show the AE hit rate and energy rate are both greater in the compression shear test compared to those in the tensile shear. This shows that the damage and destruction of the specimen is more obvious under normal compressive stress, compared to normal tensile stress. This is consistent with the observations in the previous compression shear tests, that is, the local spalling on the fractured surface and fracture damage are more obvious under compression.

4 Analysis of damage mechanisms

4.1 Time evolution of damage

Based on Martin et al.[29] and Huang et al.[10], we divide the evolution of the tensile shear and compression shear test into different damage and failure stages according to the cumulative and normalized AE hit number, as well as the shear stress−displacement. Fig.9 plots the normalized damage evolution of the specimen.

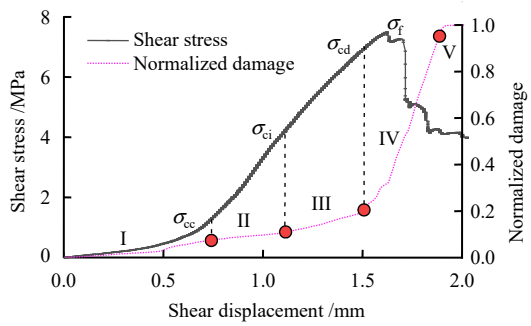

(a) Failure development under normal compression

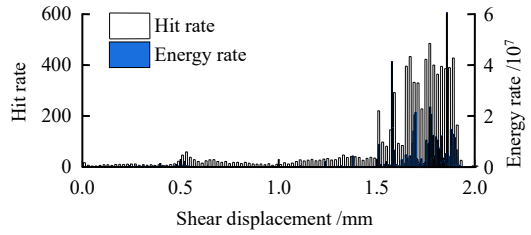

(b) Variation of AE under normal compression

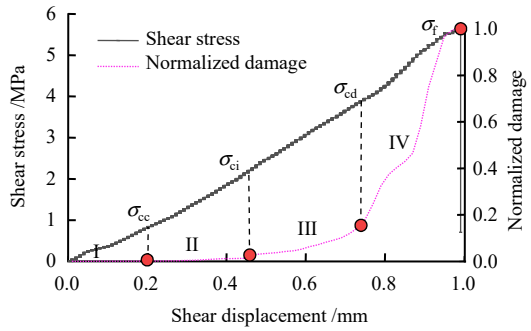

(c) failure development under normal tension

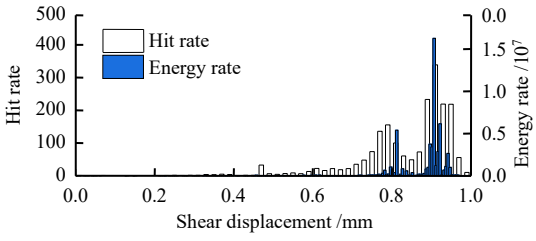

(d) Variation of AE under normal tension

Fig. 9 Plots of the development of the failure process

Figure 9(a) plots the evolution of the damage under the normal compressive stress of 3 MPa, which can be divided into five stages. The transitions between the macroscopic fracture stages of the specimen can be characterized by the shear stress critical points σ_{cc} (crack closure stress), σ_{ci} (crack initiation stress), σ_{cd} (damage stress), and σ_f (peak stress), respectively.

Crack compaction stage (I): The shear stress plot at this stage shows mainly a compaction stage, as the initial internal cracks by the shear show compactions and closures. The AE signal is weak, with only a few elastic waves being released. The corresponding critical shear stress is σ_{cc}. The cumulative hit number before this point is about 5% of the total, indicating that the damage degree of the sample is still low.

Elastic stage (II): The AE hit rate is close to zero at this stage, and almost no new cracks is generated. The specimen mainly deforms elastically, resulting in the very limited damage. The corresponding critical shear stress is σ_{ci}, which indicates the gradual development of the internal cracks at the next stage. The crack compaction stage and the elastic stage form the quiet period of the AE signal.

Crack propagation stable stage (III): The internal cracks of the sample propagate constantly at this stage, and the continuous shearing aggravates the damage of the sample. The AE hit rate increases constantly with the shear stress until the critical point of σ_{cd}, where the impact rate increases abruptly, and the damage degree of the specimen increases correspondingly. The reason could be that the cracks have propagated through the sample. Stage III is the transition stage of the AE signal, and the critical point σ_{cd} can be regarded as a precursor of the rock failure.

Crack propagation unstable stage (IV): The specimen ruptures along the preset shear plane and forms a macroscopic fracture. Multiple cracks appear on the surface, accompanied by local spalling. Meanwhile, the AE signal shows obvious activity, with the hit rate increasing rapidly until reaching its peak. During this stage, more than 70% of the hit has been counted, which results in the active period of the AE signal.

Residual stable stage (V): In this stage, the shear stress tends to be stable, and the residual stress is mainly provided by the friction of the fracture surface. Therefore, the AE signal changes from its active period with sample failure and stress drop, to a decay period with mainly constant friction. Within stage V, the hit number is about 5% of the total, indicating the damage of the specimen has gradually reached its limit.

Considering both the tensile and the compression shear tests that shown by Figs 9, the AE signals are weak in stages I and II in both of the tests, with only a few elastic waves being released. The hit rate and energy rate are both small, with almost no cracks being generated inside the sample. The degree of damage is low, which forms the quiet period of the AE signal. In particular, the AE hit rate of the tensile shear sample is even close to zero, indicating the tensile shear sample has almost no damage, compared with the greater damage degree of the compression shear test. In stage III, the hit rates of the tensile and compression shear tests both increase constantly with the shear stress, and the internal cracks of the samples have been propagating correspondingly. In comparison, the internal cracks of the compression shear specimen have expanded and connected, and the cracks are about to propagate outside the specimens; whereas the internal cracks of the tensile shear specimen have not connected and propagated that much. The AE hit rate at the critical point σ_{cd} increases abruptly. After the critical point, although the hit rate decreases a bit, the overall increase is still significant compared with the first three stages. At this time, the micro-cracks inside the sample are also developing rapidly, but the micro-cracks have not yet connected thoroughly. The "quiet" period of the hit rate during this stage forms the preparation for the subsequent connection of the micro-cracks. In Stage IV, the hit rates of the tensile and compression shear tests both increase abruptly, and the damage degree of the samples increases accordingly, which forms the active period of the AE signal. At this stage, the compression shear specimen has broken with the observation of local spalling. Many cracks appear outside the specimen. More than 70% of the hit generated during this stage. In contrast, the tensile shear specimen has not yet broken, and there is no obvious crack on the surface. However, the internal cracks of the sample at the position σ_f have been expanded and fully connected, and the damage may occur at any time with the shearing applied. More than 80% of the AE hit occurs during this stage. These observations are mainly due to the fact that for the tensile shear test, the specimen damage is dominated by the crack unstable propagation stage before the peak. The sample is separated immediately after the failure stage, and the plot shows no residual stage after the peak. Compared with the compression shear test, it can be considered that the tensile test essentially stops after the failure of the specimen. This stage can be regarded as a typical feature for the brittle failure of the tensile shear test.

The damage evolution process of the tension- and compression-shear specimens can be corresponding to the various stages of the shear stress−displacement plot, as well as the quiet period, transition period, active period and decay period represented by the cumulative hit number of the AE. The critical points σ_{cc}, σ_{ci} and σ_{cd} of the shear stress at each stage are consistent with the rock damage process characterized by the AE parameters. The critical

point σ_{cd} of the deformation plot and the b value of the AE can be used as precursors of the rock failure.

Figure 10 shows the variation of the AE hit rate under varied normal stresses. As the normal stress changes from tension to compression and increases continuously, the duration of the quiet period (stages I & II) becomes longer for the AE hit rate. As the normal stress increases, the peak stress shows a trend of increase. This indicates that due to the increase of the peak shear, the crack propagation time inside the sample is delayed correspondingly, as well as the time for the abrupt change of the hit. More time or displacement is required to initiate the AE signals and to trigger the damage of the rock. At the same time, it can also be observed that the time required for the stable and unstable crack propagation of the compression shear test is greater than that of the tensile shear test. This shows that under tension and shear stress, less time or displacement is required for the expansion and connection of the cracks inside the rock, and therefore the rate of damage and destruction is faster and more dangerous.

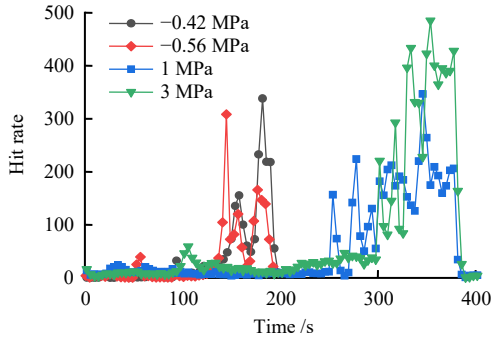

Fig. 10 Variation of the AE hit rate under different normal stress values

4.2 The forecast of failure precursor

Previous studies have shown that the b value of AE is closely related to the development of internal cracks and external macroscopic damage of rocks and concrete. In particular, for hard and brittle rocks or engineering with great potential catastrophes, the AE b value can be used to predict the dynamic disasters such as sudden rock fracture and rock burst. In this section, the AE signal during the test is analyzed to examine whether the b value is useful as an effective indicator of the rock damage.

Considering the similarity between natural earthquakes and the rock and concrete fractures, the commonly used equation in the rock and concrete field can be obtained based on the seismic frequency−magnitude (F-M) law proposed by Gutenberg et al.[30] as Eq.(3):

$$\lg N = a - b\frac{A_{dB}}{20} \quad (3)$$

where A_{dB} is the peak amplitude of the AE (dB); N is the cumulative frequency with the peak amplitude greater than A_{dB} /20; a is a value which denotes the total number of the AE hits; and b is the ratio between the small- and large-amplitude hits. The larger the b value, the fewer the large-amplitude hits.

The acquisition threshold of the AE in this test is 40 dB, that is, the signals with the peak amplitude greater than 40 dB can be monitored. As shown in Fig.11, our analysis selects the peak amplitude and frequency of the AE with a normal compressive stress of 3 MPa and a normal tensile stress of 0.42 MPa.

Each column in Fig.11(a) records the number of AE hit with a peak amplitude greater than that amplitude. For example, the first column of 3 MPa indicates that the hit number with a peak amplitude greater than 40 dB is 30 655. It shows that with the increase of the peak amplitude, the AE hit number gradually decreases. The number of hit under the normal compressive stress is much greater than that under the tensile stress. Fig.11(b) illustrates the AE signal as a whole, and evaluates the b value by linear regression. It is clearly shown by the figure that the AE b value is closely related to the total hit number N, as well as the high-amplitude hits.

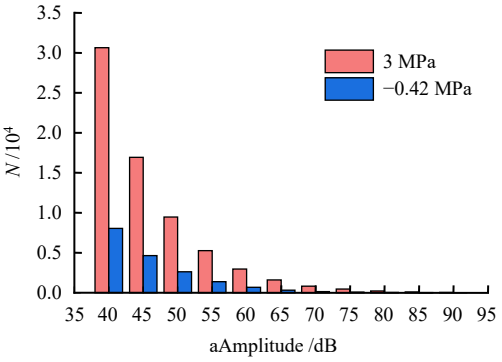

(a) Cumulative distribution of amplitude

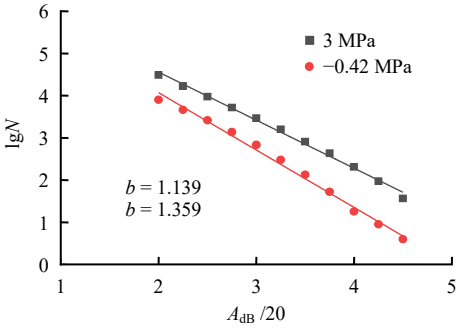

(b) Fit of the AE amplitude

Fig. 11 Variation between the AE peak amplitude and frequency

As shown by Fig.12, the AE b value in the tensile stress region is significantly greater than that in the compressive region. This is mainly because, the internal and external cracks develop completely compared with the tensile shear failure, and the local spalling phenomenon appears significantly after the fracture when the specimen is subjected to compressive shear stress. The number of

large-amplitude AE hits increases significantly; the large-to-small ratio of hits also increases; and the *b* value decreases significantly. These observations are consistent with the features of the two fracture surfaces described above.

The relationship between the AE *b* value and the normal stress is obtained by the fitting of logarithmic regression: $b = 1.134 + 0.312 \times 0.304^{\sigma_n}$, with $R^2 = 0.724$. As shown by the fitted plot, the AE *b* value decreases with the increase of the normal stress, indicating that the greater the normal stress is, the more obvious the damage behaves.

Based on the above analysis, the *b* value of AE decreases continuously during the failure, and the *b* value decreases with the increase of normal stress. Due to the fact that a smaller *b* value is related to a greater rock burst, it means that the larger the normal stress, the more obvious the rock burst during the failure. Therefore, the AE *b* value can be used as an indicator to predict the degree of rock damage.

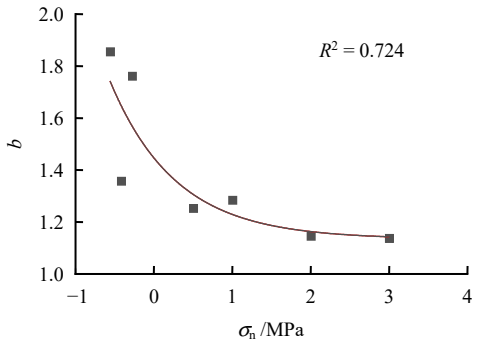

Fig. 12 Variation of the AE *b* value with the normal stress

5 Conclusion

This paper presents a design of an auxiliary device for the tensile shear test. The deformation mechanism and the mechanical properties of the specimens are studied under different normal stress conditions by using the device. At the same time, AE was used to record the hit, amplitude, energy and other signals of the specimen during the shearing process, based on which the damage mechanism of the specimen and the prediction of precursors was studied. The main conclusions are listed as follows.

(1) The stress in the post-peak phase of the tensile shear sample drops rapidly and the specimen quickly separates into two parts. Compared with the compression shear stress that falls to the residual stage after the peak, the tensile shear failure exhibits more brittle failure.

(2) The appearance of the fracture surface of the sample is closely related to the direction and the magnitude of the normal stress. In general, the larger the normal compressive stress is, the larger the area of the sample friction zone becomes, and the more obvious the local spalling phenomenon behaves. Compared with compression shear, the friction zone of the fracture surface and the spalling of the specimen are not obvious under the tensile shear stress.

(3) The peak stress is more sensitive to the normal tensile stress, and the relation is more complicated. The Mohr-Coulomb strength criterion lacks the ability to fit the tensile stress area. The Hoek-Brown strength criterion can generally capture the strength characteristics of the full stress zone.

(4) The variations of hit rate and energy rate are similar for both the compression- and tension-shear tests. They both increase first and then decrease with the change of shear stresses. They both have small values before the peak and increase rapidly at or near the peak stress. The tensile shear test curve lacks the post-peak phase. Before the broken of the specimen, the hit rate remains at a high level. The hit and energy rate of the compression shear test are greater than those of the tensile shear, and the damage and destruction are more obvious.

(5) The normalized cumulative AE hit number can be used to characterize the damage degree of the specimen and its damage evolution process. The crack compaction stage and elastic stage of the tension- and compression-shear tests have shown subtle damage, and contribute to the quiet period of the AE signal. The duration of the period becomes longer as the normal stress increases. The damage in the tensile shear test is dominated by the pre-peak stage, whereas for the compression shear it is dominated by the post-peak stage. Moreover, the rate of damage at each stage of the tensile shear test is faster as shown by the plot, and the test essentially stops after the sample is broken. These observations should be related to the brittleness of the failure behavior.

(6) The shear stress critical points σ_{cc}, σ_{ci} and σ_{cd} at each stage can be used to characterize the macroscopic fracture of the sample, which is consistent with the microscopic fracture of the sample that characterized by the AE parameters. The AE *b* value decreases continuously during the sample being damaged, and it decreases with the increase of the normal stress. The *b* value can be used as a precursor for the rock failure together with the critical point σ_{cd}.

References

[1] HUANG R Q, HUANG D. Evolution of rock cracks under unloading condition[J]. Rock Mechanics and Rock Engineering, 2014, 47(2): 453−466.

[2] HUANG R Q, WANG X N, CHAN L S. Triaxial unloading test of rocks and its implication for rock burst[J]. Bulletin of Engineering Geology and the Environment, 2001, 60(1): 37−41.

[3] LI Di-yuan, LI Xi-bing, CHARLIE Li-c. Experimental studies of mechanical properties of two rocks under direct compression and tension[J]. Chinese Journal of Rock

Mechanics and Engineering, 2010, 29(3): 624−632.

[4] YU Xian-bin, WANG Qing-rong, LI Xin-yi, et al. Experimental research on deformation of rocks in direct tension and compression[J]. Rock and Soil Mechanics, 2008, 29(1): 18−22.

[5] YU Xian-bin, XIE Qiang, LI Xin-yi, et al. Cycle loading tests of rock samples under direct tension and compression and bi-modular constitutive model[J]. Chinese Journal of Geotechnical Engineering, 2005, 27(9): 988−993.

[6] RAMSEY J M, CHESTER F M. Hybrid fracture and the transition from extension fracture to shear fracture[J]. Nature, 2004, 428: 63−66.

[7] ZHOU Huo-ming, XIONG Shi-hu, LIU Xiao-hong, et al. In-situ tension-shear tests and strength criterion studies on tgp shiplock slope rockmass[J]. Chinese Journal of Rock Mechanics and Engineering, 2005, 24(24): 4418−4421.

[8] KONG Xiao-ang, CAI Guo-qing, LIU Zhen-zhen, et al. Research on tensile-shear coupling strength of unsaturated clays[J]. Rock and Soil Mechanics, 2017, 38(Suppl.2): 9−17.

[9] KONG Xiao-ang, CAI Guo-qing, ZHAO Cheng-gang. Study on tenso-shear coupling strength of clays[J]. Rock and Soil Mechanics, 2016, 37(8): 2285−2292.

[10] HUANG D, CEN D F, SONG Y X. Comparative investigation on the compression-shear and tension-shear behaviour of sandstone at different shearing rates[J]. Rock Mechanics and Rock Engineering, 2020, 53(1). DOI: 10.1007/S00603-020-02094-3.

[11] CEN Duo-feng, LIU Chao, HUANG Da. Experimental and numerical study on tensile-shear strength and rupture characteristics of sandstone[J]. Chinese Journal of Rock Mechanics and Engineering, 2020, 39(7): 1333−1342.

[12] HUANG Da, ZHANG Yong-fa, ZHU Tan-tan, et al. Experimental study on tension-shear mechanical behavior of sandstone[J]. Chinese Journal of Geotechnical Engineering, 2019, 41(2): 272−276.

[13] CEN D F, HUANG D. Direct shear tests of sandstone under constant normal tensile stress condition using a simple auxiliary device[J]. Rock Mechanics and Rock Engineering, 2017, 50(6): 1425−1438.

[14] CHEN J, ZHOU H, ZENG Z Q, et al. Macro- and microstructural characteristics of the tension–shear and compression-shear fracture of granite[J]. Rock Mechanics and Rock Engineering, 2020, 53(1): 201−209.

[15] MENG Q B, ZHANG M W, HAN L J, et al. Acoustic emission characteristics of red sandstone specimens under uniaxial cyclic loading and unloading compression[J]. Rock Mechanics and Rock Engineering, 2018, 51(4). DOI: 10.1007/S00603-017-1389-6.

[16] MENG Q B, ZHANG M W, HAN L J, et al. Effects of acoustic emission and energy evolution of rock specimens under the uniaxial cyclic loading and unloading compression[J]. Rock Mechanics and Rock Engineering, 2016, 49(10): 3873−3886.

[17] LI L R, DENG J H, ZHENG L, et al. Dominant frequency characteristics of acoustic emissions in white marble during direct tensile tests[J]. Rock Mechanics and Rock Engineering, 2017, 50(5). DOI: 10.1007/S00603-016-1162-2.

[18] CHEON D S, JUNG Y B, PARK E S, et al. Evaluation of damage level for rock slopes using acoustic emission technique with waveguides[J]. Engineering Geology, 2011, 121(1-2): 75−88.

[19] MENG F Z, WONG L N Y, ZHOU H, et al. Asperity degradation characteristics of soft rock-like fractures under shearing based on acoustic emission monitoring[J]. Engineering Geology, 2020, 266. DOI: 10.1016/j.enggeo.2019-105392.

[20] ZHANG Yan-bo, WU Wen-rui, YAO Xu-long, et al. Acoustic emission, infrared characteristics and damage evolution of granite under uniaxial compression[J]. Rock and Soil Mechanics, 2020, 41(Suppl.1): 139−146.

[21] LIU Xi-ling, LIU Zhou, LI Xi-bing, et al. Acoustic emission *b*-values of limestone under uniaxial compression and Brazilian splitting loads[J]. Rock and Soil Mechanics, 2019, 40(Suppl.1): 267−274.

[22] CHEN N, ZHANG X B, JIANG Q H, et al. Shear behavior of rough rock joints reinforced by bolts[J]. International Journal of Geomechanics, 2017, 18(1). DOI: 10.1061/CAS(E)GM.1943-5622.0001048.

[23] ZHANG X B, JIANG Q H, CHEN N, et al. Laboratory investigation on shear behavior of rock joints and a new peak shear strength criterion[J]. Rock Mechanics and Rock Engineering, 2016, 49(9). DOI: 10.1007/S00603-016-1012-2.

[24] LI Ping-en, YIN You-quan. Modification of drucker-prager criterion in tensile shear region[J]. Chinese Journal of Rock Mechanics and Engineering, 2010, 29(Suppl.1): 3029−3033.

[25] ZHOU Hui, LU Jing-jing, XU Rong-chao, et al. Research on tension-shear failure characteristics and yield criterion of hard brittle marble[J]. Rock and Soil Mechanics, 2016, 37(2): 305−314.

[26] LI Shou-ding, LI Xiao, GUO Jing-yun, et al. Research of rock failure testing under combined shear and tension[J]. Journal of Engineering Geology, 2014, 22(4): 655−666.

[27] LIU Fu-zheng. Study on mechanical property of rock in tension and tension-shear state[J]. Journal of Yangtze River Scientific Research Institute, 1996(3): 38−42.

[28] MENG F Z, ZHOU H, WANG Z Q, et al. Experimental study on the prediction of rockburst hazards induced by dynamic structural plane shearing in deeply buried hard rock tunnels[J]. International Journal of Rock Mechanics and Mining Sciences, 2016, 86: 210−223.

[29] MARTIN C D, CHANDLER N A. The progressive fracture of Lac du Bonnet granite[J]. International Journal of Rock Mechanics and Mining Sciences & Geomechanics Abstracts, 1994, 31(6): 643−659.

[30] GUTENBERG B, RICHTER C F. Frequency of earthquakes in California[J]. Nature, 1945, 156(3960): 371.